Int. J. Heat Mass Transfer. Vol. 36, No. 11, pp. 2899–2911, 1993
Printed in Great Britain

0017-9310/93 $6.00+0.00

Numerical study of laminar and turbulent natural convection in an inclined square cavity

R. A. KUYPER, TH. H. VAN DER MEER, C. J. HOOGENDOORN
and R. A. W. M. HENKES

Faculty of Applied Physics, Delft University of Technology, Lorentzweg 1, 2628 CJ Delft,
The Netherlands

(*Received* 18 *May* 1992)

Abstract—Two-dimensional numerical simulations of the natural convection flow of air in a differentially heated, inclined square cavity were performed for both laminar and turbulent flows. The angle of inclination of the cavity was varied from 0° (heated from below) to 180° (heated from above). For Rayleigh numbers between 10^4 and 10^{11} the natural convection flow has been calculated. A detailed analysis was made for Rayleigh numbers of 10^6 and 10^{10}. The standard k–ε model for turbulence was used in the prediction of turbulent flows. Numerical predictions of the heat flux at the hot wall and the influence of the angle of inclination on the Nusselt number are presented. The Nusselt number shows strong dependence on the orientation of the cavity and the power law dependence on the Rayleigh number of the flow. Flow patterns and isotherms are shown to give greater understanding of the local heat transfer. For the high Rayleigh number calculations hysteresis of the solution was found at a transition of flow patterns.

1. INTRODUCTION

THE STUDY of the natural convection flow in a cavity has mainly been devoted to the two limiting situations of the Rayleigh–Bénard problem, where the gravitational vector is parallel to the imposed temperature gradient, and the configuration of a cavity heated from the vertical side. Especially, numerical calculations of natural convection flow in the turbulent regime have been limited to these two cases [1]. However, in many applications the position of the hot and cold wall of a cavity with respect to the gravitational vector demands a study in which buoyancy forces have both normal and tangential components relative to the cavity walls. The present study provides numerical simulations of the natural convection flow in a wide variety of orientations and Rayleigh numbers.

The significance of the research on natural convection flow in inclined cavities has been discussed in review articles of Yang [1] and Catton [2]. Though the majority of studies are dedicated to the two extreme situations, comprehension of these flows may be enlarged by considering them as merely one of the many flow patterns appearing in changing the cavity orientation.

In the early 1970s, the first thorough studies of natural convection in inclined cavities appeared and were dedicated to the stability problem of the flow. Hart [3] determined the critical Rayleigh number and the associated flow patterns for the instabilities of an inclined heated flat plate. Following this qualitative approach, a number of studies were dedicated to the experimental determination of Nusselt numbers for laminar flows in inclined cavities of large aspect ratio. These studies arose from the intensive investigation of the application of solar energy collectors and double-glazed windows. Up to the 1980s, experimental research was performed on determination of Nusselt numbers (e.g. [4–6]), flow structures (e.g. [7]) and critical Rayleigh number (e.g. [8]).

Also in the numerical determination of the natural convection flow in inclined cavities, research was focused on laminar flows and on the early stages of its transition to turbulence. Ozoe *et al.* [9, 10] and Catton *et al.* [11] performed studies on the numerical approach of this subject.

In the 1980s, the knowledge of the flows was extended by numerical investigation of the 3D aspects [12] and the influence of variable fluid properties and radiation [13]. Local heat-transfer measurements and calculations were recently reported by Hamady *et al.* [14]. We might say that nowadays the laminar regime in natural convection in inclined enclosures is quite well known.

During the last few years, the subject of natural convection in inclined cavities has been extended by additional variations. Research has been done on the influence of partitions in the geometry, on changes in the geometry (e.g. [15, 16]) and on changes in the boundary conditions, for example cavities heated by two perpendicular walls.

Except for the two limiting situations (e.g. [17, 18]) and some orienting work by Lankhorst [19], high Rayleigh number turbulent natural convection in the inclined cavity has so far been neglected. Experimentally, the heat transfer has been examined up to $Ra = 10^8$ [20], but numerical analysis for turbulent flows in inclined enclosures has not been reported on.

This study will give results in both the laminar and the turbulent regime. Besides the similarities between

NOMENCLATURE

a	thermal diffusivity [$m^2 s^{-1}$]
$C_\mu, c_{\varepsilon 1}, c_{\varepsilon 2}, c_{\varepsilon 3}$	factors in k–ε model, see equation (5)
g	gravitational acceleration [$m s^{-2}$]
G_k	buoyancy term in equations (4) and (5)
H	cavity height = cavity width [m]
k	turbulent kinetic energy [$m^2 s^{-2}$]
Nu	local Nusselt number, equation (7)
$\overline{Nu}$	mean Nusselt number, equation (7)
p	pressure [Pa]
P_k	production term in equations (4) and (5)
Pr	Prandtl number, see equation (6)
Ra	Rayleigh number, see equation (6)
t	time [s]
T	temperature [K]
u, v	velocity components in the x-, y-direction
x, y	coordinates in the x-, y-direction.

Greek symbols

β	volumetric thermal expansion coefficient [K^{-1}]
ε	turbulent energy dissipation rate [$m^2 s^{-3}$]
θ	angle between $\vec{u}$ and $\vec{g}$
ρ	density [$kg m^{-3}$]
σ	turbulent Prandtl number
φ	angle of inclination, see Fig. 1 [deg].

Subscripts

C	cold wall
H	hot wall
i	coordinate index
t	turbulent quantity
1, 2	coordinate indices.

Superscript

$\vec{\ }$	vector indicator.

the two situations, some remarkable phenomena in the turbulent flows will be presented.

2. MATHEMATICAL FORMULATION

The geometry of a two-dimensional cavity is shown in Fig. 1. This study has been limited to a square cavity filled with air. The walls at $x = 0$ and H are differentially heated with the hot surface at $x = 0$. The surfaces at $y = 0$ and H are insulated. The angle of inclination φ is defined by the angle between the hot wall and the horizontal, in which case $\varphi = 0$ is the situation of a cavity heated from below. Radiation effects are neglected, the fluid is assumed to be incompressible and the Boussinesq approximation is assumed to be valid [21].

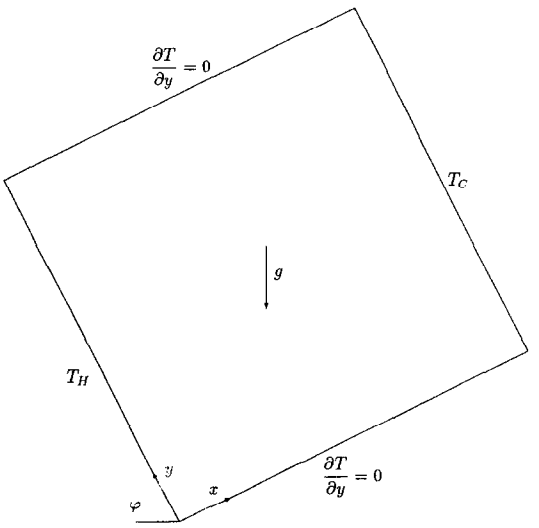

FIG. 1. Model of the cavity geometry.

The natural convection flow is described by the equations of conservation of mass, momentum and energy. In order to describe turbulent flows, the standard k–ε model for the turbulent kinetic energy and its dissipation is used (e.g. [22]). The following set of equations, the Reynolds equations, has now been obtained

$$\vec{\nabla} \cdot \vec{u} = 0 \tag{1}$$

$$\frac{\partial u}{\partial t} + \vec{\nabla} \cdot \vec{u}u = -\frac{1}{\rho}\frac{\partial p}{\partial x} - g_1 \beta (T - T_0) + \vec{\nabla} \cdot (\nu + \nu_t)\vec{\nabla}u + \vec{\nabla} \cdot (\nu + \nu_t)\frac{\partial \vec{u}}{\partial x} \tag{2a}$$

$$\frac{\partial v}{\partial t} + \vec{\nabla} \cdot \vec{u}v = -\frac{1}{\rho}\frac{\partial p}{\partial y} - g_2 \beta (T - T_0) + \vec{\nabla} \cdot (\nu + \nu_t)\vec{\nabla}v + \vec{\nabla} \cdot (\nu + \nu_t)\frac{\partial \vec{u}}{\partial y} \tag{2b}$$

$$\frac{\partial T}{\partial t} + \vec{\nabla} \cdot \vec{u}T = \vec{\nabla} \cdot \left(\frac{\nu}{Pr} + \frac{\nu_t}{\sigma_T}\right)\vec{\nabla}T \tag{3}$$

$$\frac{\partial k}{\partial t} + \vec{\nabla} \cdot \vec{u}k = \vec{\nabla} \cdot \left(\nu + \frac{\nu_t}{\sigma_k}\right)\vec{\nabla}k + P_k + G_k - \varepsilon \tag{4}$$

$$\frac{\partial \varepsilon}{\partial t} + \vec{\nabla} \cdot \vec{u}\varepsilon = \vec{\nabla} \cdot \left(\nu + \frac{\nu_t}{\sigma_\varepsilon}\right)\vec{\nabla}\varepsilon + (c_{\varepsilon 1}(P_k + c_{\varepsilon 3}G_k) - c_{\varepsilon 2}\varepsilon)\frac{\varepsilon}{k} \tag{5}$$

in which

$$\nu_t = C_\mu \frac{k^2}{\varepsilon}, \quad P_k = \nu_t\left(2\nabla\vec{u}\cdot\nabla\vec{u} + \left(\frac{\partial u}{\partial y} + \frac{\partial v}{\partial x}\right)^2\right),$$

$$G_k = \frac{\nu_t}{\sigma_T}\vec{g}\cdot\beta\vec{\nabla}T.$$

The vector $\vec{g}$ has components $\vec{g} = (g_1, g_2) = (-g\cos\varphi, -g\sin\varphi)$. Laminar flows are described by setting $\nu_t = 0$ in the equations and omitting the equations for k and ε.

The following constants are used in the k–ε model

$$C_\mu = 0.09, \quad c_{\varepsilon 1} = 1.44, \quad c_{\varepsilon 2} = 1.92,$$

$$\sigma_T = 1.0, \quad \sigma_k = 1.0, \quad \sigma_\varepsilon = 1.3.$$

The buoyancy factor $c_{\varepsilon 3}$ is taken as

$$c_{\varepsilon 3} = \tanh\left(\frac{|\vec{g}\cdot\vec{u}|}{\sqrt{(|\vec{g}|^2|\vec{u}|^2 - |\vec{g}\cdot\vec{u}|^2)}}\right) = \tanh|\cot(\theta)|$$

in which θ is the angle between $\vec{g}$ and $\vec{u}$, in order to be close to 1 in the vertical part of boundary layers and close to 0 in the horizontal part.

At the walls, zero velocities are prescribed and the boundary conditions for the temperature equation are taken as shown in Fig. 1. The equations for k and ε have been solved using two kinds of boundary conditions. The first set of boundary conditions, originally derived for forced convection boundary layer flow, applies wall functions in order to reduce the number of grid points within the boundary layer. At the first inner grid point, the turbulent kinetic energy and its dissipation are given by the values

$$k = \frac{u_\tau^2}{\sqrt{C_\mu}}, \quad \varepsilon = \frac{u_\tau^4}{0.41\nu y^+}$$

in which the dimensionless variable $y^+ = y_n u_\tau/\nu$ and the scaled variable $u_\tau = \sqrt{(\nu(\partial u_t/\partial y_n))}$ appear (y_n is the distance to the closest wall and u_t the velocity component tangential to that wall). In order to avoid the requirements of this set of boundary conditions with respect to the positioning of the first inner grid point, a second type of boundary conditions has been used by taking $k = 0$ and $\varepsilon = \infty$ at the walls [22]. The turbulent Prandtl number is changed to $\sigma_T = 0.9$ when using these Dirichlet conditions. Both sets of boundary conditions have been used in this study. The main results have been obtained by using the first set of boundary conditions, while the second set of boundary conditions has been used to compare the obtained flow characteristics and heat transfer results qualitatively.

The solution of equations (1)–(5) is fully determined by three parameters: the Rayleigh number Ra, the Prandtl number Pr and the angle of inclination φ, where Ra and Pr are defined by

$$Ra = \frac{g\beta\Delta T H^3}{\nu a}, \quad Pr = \frac{\nu}{a}. \tag{6}$$

We have used a Prandtl number of 0.71 in solving the equations and we are mainly interested in the dependence of the angle of inclination in two regimes: in the laminar regime solutions were obtained for $Ra = 10^6$ and in the turbulent regime we used $Ra = 10^{10}$. The calculated heat transfer at the wall is presented by the local Nusselt number Nu and the averaged Nusselt number $\overline{Nu}$, which are defined as

$$Nu = -\frac{H}{\Delta T}\left(\frac{\partial T}{\partial x}\right)_{x=0}, \quad \overline{Nu} = \frac{1}{H}\int_{y=0}^{H} Nu\,dy. \tag{7}$$

3. NUMERICAL PROCEDURE

Equations (1)–(5) are solved using a finite-volume method with a pressure-correction method as introduced by Patankar and Spalding [23]. After each line Gauss–Seidel sweep for the momentum, energy and turbulence equations, the Poisson equation for the pressure correction was solved directly over the full domain. Although we are interested in stationary solutions, the time-dependent formulation was used in the discretization of the equations in order to better describe the physical process of rotating the cavity and to provide a good tool to control convergence.

The convection–diffusion terms in equations (2)–(5) were discretized using the central scheme in laminar calculations and the hybrid scheme in turbulent flow problems. Our numerical results for the case $\varphi = 90°$ were already compared with the laminar benchmark solutions of de Vahl Davis [24] and the turbulent solutions of Markatos and Pericleous [17] in a previous study [22].

Because of the symmetrical properties of the steady solution, if we take $T_0 = (T_H + T_C)/2$, it is possible to solve the equations on half the domain $0 \leqslant x \leqslant H/2$. On $x = H/2$ the boundary conditions then read $u(y) = -u(H-y)$, $v(y) = -v(H-y)$, $p(y) = p(H-y)$, $T(y) = 1 - T(H-y)$, $k(y) = k(H-y)$ and $\varepsilon(y) = \varepsilon(H-y)$. This roughly reduces computational time by a factor of 2. In order to obtain a sufficient number of grid points in the boundary layers, grid points were positioned using a sinusoidal distribution according to

$$\frac{x_i}{H} = \frac{i}{N} - \frac{1}{2\pi}\sin\left(2\pi\frac{i}{N}\right) \quad \text{for} \quad i = 1, \ldots, N$$

in both the x- and y-direction.

Three criteria were used to check convergence: the net heat flux through the cavity walls should be small, the net mass flow through half the cavity height should be small and the computed variables should change little during a sweep and a time step. Grid refinement was applied to check the accuracy of the solution. The number of grid cells used in the calculations were chosen such that doubling the number of cells changed the mean Nusselt number by less than 5%. In most calculations 60×60 grid points were used to obtain this accuracy.

4. RESULTS

4.1. *Flow characteristics*

Two interesting phenomena in heat transfer are associated with the inclination of a differentially heated cavity. For low Rayleigh number situations, as well as for angles of inclination close to 180°, conduction of heat through the air layer dominates the heat transfer and the flow of the fluid is limited. In other cases the fluid motion may become the dominating factor in heat transfer.

For three situations, the flow structure is quite well known. Heated from above ($\varphi = 180°$), the fluid theoretically stands still and the Nusselt number is purely determined by conduction: $Nu = 1$. The flow in a cavity heated from the side ($\varphi = 90°$) at sufficiently high Rayleigh number is dominated by the thoroughly investigated natural convection boundary layer flow along the hot and cold wall. Further rotation at the same Rayleigh number gives rise to higher velocities because of the increasingly unstable situation of a cavity heated from below. For $\varphi = 0°$, the flow is three-dimensional for Rayleigh numbers sufficiently high and cannot be described by the two-dimensional

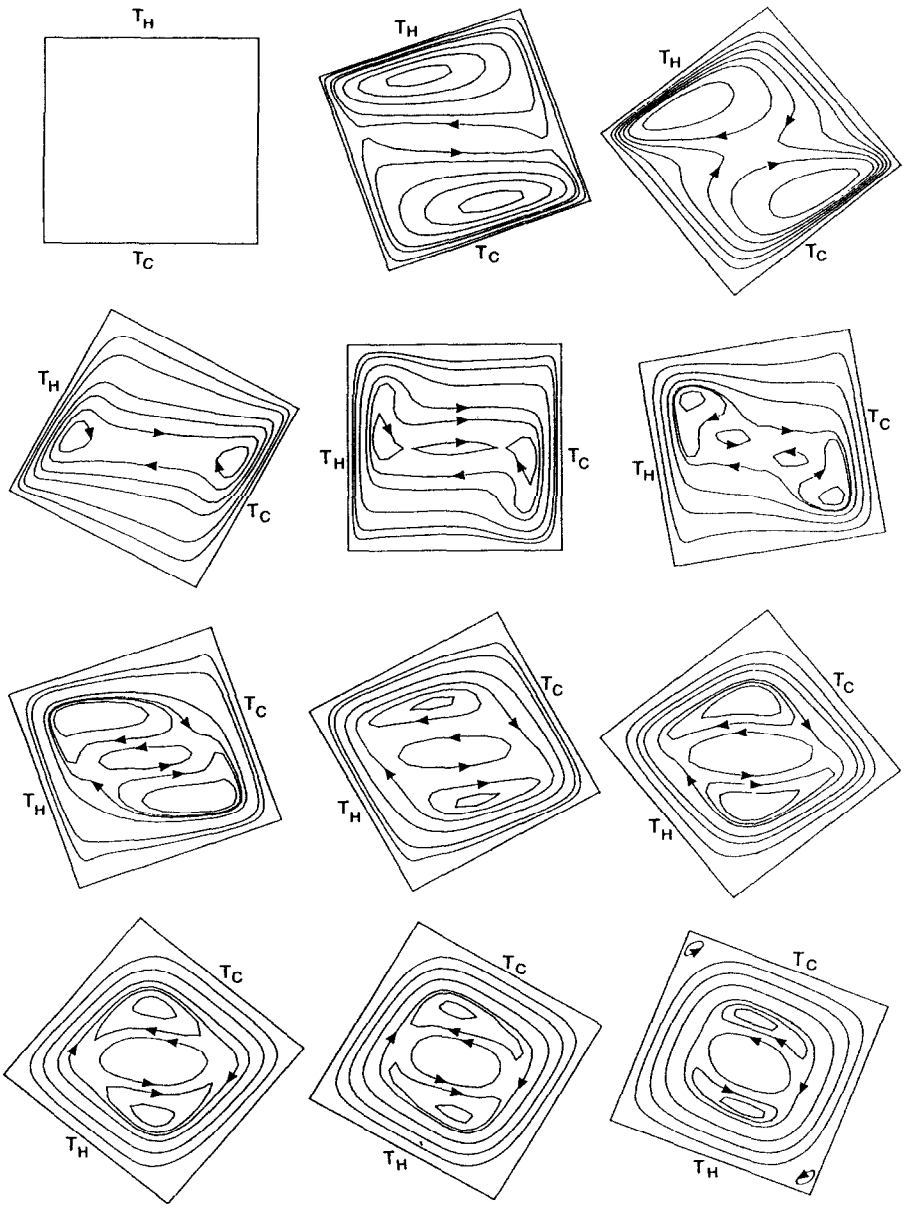

FIG. 2. Flow fields for $Ra = 10^6$. Plotted are some isolines of the streamfunction for $\varphi = 180°$, $\varphi = 160°$, $\varphi = 140°$, $\varphi = 120°$, $\varphi = 90°$, $\varphi = 80°$, $\varphi = 70°$, $\varphi = 60°$, $\varphi = 50°$, $\varphi = 40°$, $\varphi = 30°$, $\varphi = 20°$.

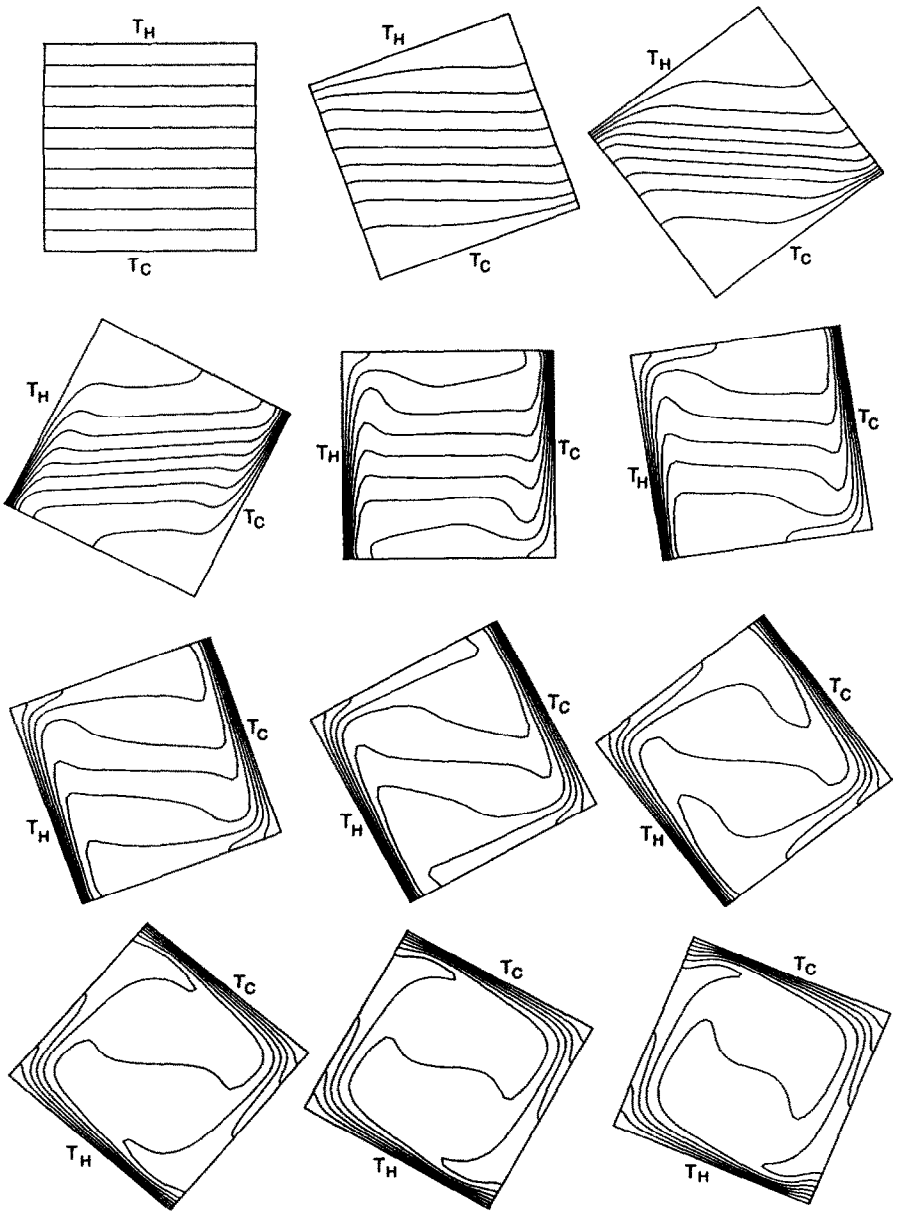

FIG. 3. Temperature distribution for $Ra = 10^6$. Plotted are isotherms $(T-T_C)/\Delta T = 0(0.1)1$ at angles $\varphi = 180°$, $\varphi = 160°$, $\varphi = 140°$, $\varphi = 120°$, $\varphi = 90°$, $\varphi = 80°$, $\varphi = 70°$, $\varphi = 60°$, $\varphi = 50°$, $\varphi = 40°$, $\varphi = 30°$, $\varphi = 20°$.

numerical program. The transitions between these flow regimes will be discussed for both laminar flows ($Ra = 10^6$) and turbulent flows ($Ra = 10^{10}$).

4.2. *Laminar flow*

According to the combined experimental and numerical study of Hamady *et al.* [14], the flow at a Rayleigh number of 10^6 and an aspect ratio of one is two-dimensional and laminar for an angle of inclination larger than approximately 25°. In the present study, steady two-dimensional results could be obtained up to a minimal angle of 20°. Since convergence was significantly slowing down approaching this angle, the highly unstable and probably three-dimensional flow at smaller angles was not considered.

In Fig. 2, the calculated flow fields are plotted for angles of inclination of 20 to 180°. The flow fields are visualized by a few streamlines, which show the topology of the flow. In Fig. 3, the associated temperature distribution is plotted for isotherms of $(T-T_C)/\Delta T = 0(0.1)1$. We will discuss the change in velocity and temperature fields under rotation of the cavity from 180 to 20°. In Fig. 4 the local Nusselt

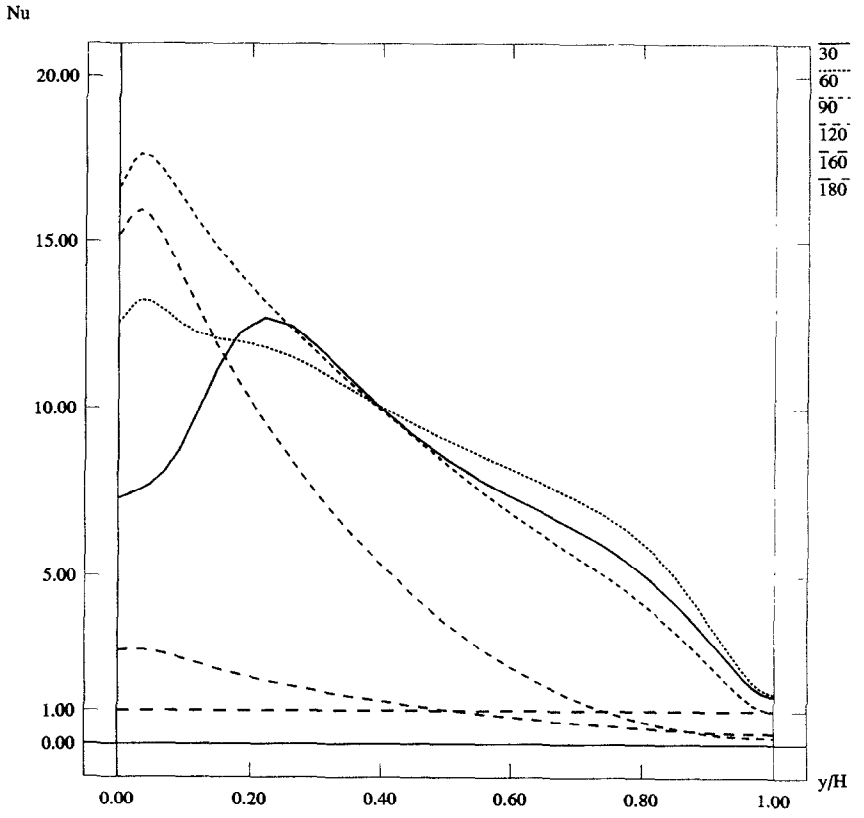

FIG. 4. Local Nusselt number distribution at some angles of inclination for $Ra = 10^6$.

number distribution along the hot wall is given for some angles of inclination. Figure 5 shows the averaged Nusselt number distribution at different angles of inclination of the cavity.

At $\varphi = 180°$, the calculated flow and temperature distribution confirm the theoretical prediction of a situation fully determined by diffusion. There is no flow and the small cells appearing in the experimental study of Hamady *et al.* [14] indicate that their connecting walls are not perfectly insulated. The local Nusselt number along the hot wall and the mean Nusselt number equal unity. As soon as the cavity is rotated to $\varphi = 160°$, the fluid is set in motion. At first little mass reaches the opposite wall; fluid leaving the heated or cooled wall is returning to the same wall, forming a stretched cell along both walls. The isotherms in the core remain oriented perpendicular to the gravitational vector during rotation. Rotating the cavity to $\varphi = 140°$, decreases the size of the cells along the heated and cooled wall, since an increasing part of the fluid reaches the opposite side. The velocities along the hot and cold wall increase under rotation, but since the air leaving the hot wall is relatively hot, it will move quite slowly on its way 'down' to the cold wall since $\varphi > 90°$. The temperature gradient in the core region gets larger. Since hot fluid is positioned in the upper corner and cold air in the lower corner, diffusion is still the dominating process in the cavity. In fact, for angles of inclination larger than 90° the local Nusselt number distribution shows values smaller than 1 at the upper part of the hot wall. For angles closer to 90°, most of the fluid leaving the hot wall is no longer decelerated due to gravity and reaches the cold wall, producing the rapid growth of the mean Nusselt number as indicated by Fig. 5.

The essential part of the flow at 90° is the vertical boundary layer structure along the hot and cold surfaces. At the corner regions the boundary layer hits the adiabatic walls and spreads to a wide non-accelerating horizontal flow. Along the boundary layers, a small portion of the fluid is entering the boundary layer upstream again, forming the same narrow cell as in the case of $\varphi > 90°$. In the core of the cavity, the flow is stably stratified: velocities are perpendicular to the gravitational field and the temperature increases with the height.

Rotating the cavity hot wall to a smaller angle of $\varphi = 80°$ produces an acceleration of the flow along the top and bottom wall. The narrow cells are stretched along these walls and will dominate an increasing part of the core region flow, while the flow along these walls remains perpendicular to the gravitational field. The entrainment of cold fluid in the boundary layer at the hot wall is spread over a larger part of the

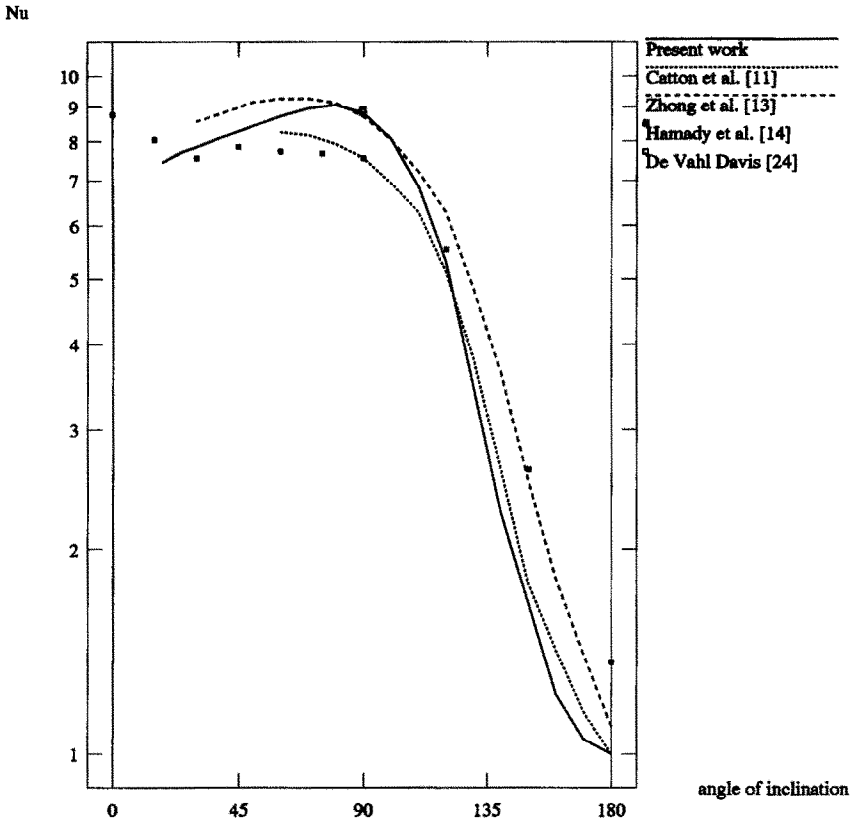

FIG. 5. Dependence of mean Nusselt number on angle of inclination for $Ra = 10^6$.

hot wall boundary layer, thereby smoothing the local Nusselt number distribution.

Further rotation to $\varphi = 70°$, makes the corner region cells spread towards the opposing walls, as the velocity along the adiabatic walls increases. The highest velocities in the cavity now appear along these walls instead of in the hot and cold wall boundary layers. As the cell reaches the opposing boundary layer at $\varphi = 60°$, mass will leave this layer perpendicular to the gravitational field to feed the cell. The two cells are starting to interact, forming a counterclockwise rotating closed cell in the centre of the cavity. The flow in this core region pushes the flow along the adiabatic walls to the side, breaking up the temperature stratification in the core. Because of the good mixing now obtained in the core, temperature gradients are small here.

At an angle of inclination of 40°, the cell at the lower end of the hot wall will feed relatively cold air to the hot-wall side of the centre region, while the cell at the upper part of the cold wall feeds relatively hot air to the cold-wall side. In this way the counterclockwise rotation of the cell in the centre is accelerated, bending the isotherms in the centre such that they are no longer orthogonal to the gravitational field. The size of this cell increases, squeezing the two original cells towards the hot and cold wall boundary layers. At $\varphi = 20°$ the flow shows three regions:

- the main flow is moving along the hot and cold wall and leaves the adiabatic side walls before it reaches the isotherm walls;
- the core region contains a counterclockwise rotating cell, growing under further rotation and approaching the main flow;
- the regions at the start of the boundary layers of the hot and cold wall are occupied by small counterclockwise rotating cells. This can already be seen from the local minimum in the local Nusselt number distribution at an angle of inclination of 30° in Fig. 5.

The clockwise and counterclockwise rotating cells in the core are now starting to interact on a small area and further rotation makes the flow structure increasingly unstable. Close to this angle of inclination there will probably be a transition to a three-dimensional flow.

The calculated mean Nusselt number as a function of φ is plotted in Fig. 5. In this figure, the numerical results of Catton *et al.* [11] using a Galerkin method, the experimental results of Hamady *et al.* [14], the numerical results of Zhong *et al.* [13] and the benchmark solution of de Vahl Davis at $\varphi = 90°$ [24] are included. The function shows a maximum and a local minimum. The maximum Nusselt number has been obtained at an angle of 80°, the minimum was found

at the smallest converged angle. As the study of Hamady *et al.* concluded, the minimum is associated with the transition at $\varphi \approx 20°$. Compared with the results of previous studies in the laminar regime, our results show close agreements. The difference with the result of Hamady *et al.* [14] is due to the conduction through the connecting walls in their experiments. Zhong *et al.* [13] included variable properties in their calculations, leading to differences in those situations where heat is mainly transported by diffusion: at $\varphi = 180°$ they calculated a Nusselt number larger than unity. The results of Catton *et al.* [11] do have $Nu = 1$ at $\varphi = 180°$, but their maximum in the mean Nusselt number is too low when compared to the benchmark solution of de Vahl Davis [24].

4.3. *Turbulent flow*

The results for $Ra = 10^{10}$ can be divided into two numerical regimes. Using a hybrid scheme, laminar solutions could be obtained for angles of inclination larger than 90°, for other angles turbulent calculations were made. Close to an angle of inclination of 90° both the laminar and the turbulent calculations converged to approximately the same result. Although the physical situation of a cavity heated from above is stable, the calculations converged rather slow for angles of inclination larger than 90°. Since the calculated flow patterns and temperature distribution for angles of inclination larger than 90° do not differ much from the case $Ra = 10^6$, we will only discuss the results for rotating the cavity from 90 to 30°.

Figure 6 shows the flow structures, visualized by some streamlines. Figure 7 shows the associated temperature distribution and Fig. 8 gives the calculated mean Nusselt number as a function of the angle of inclination.

At $\varphi = 90°$ the flow is dominated by thin boundary layers along the hot and cold wall. The velocity and temperature distribution in a large part of the cavity is extremely well stratified. At a Rayleigh number of 10^{10}, the slightest rotation disturbs the flow along the adiabatic walls, while at $Ra = 10^6$, results at $\varphi = 90°$ do not change abruptly under rotation.

At 80°, the flow in the core is still persisting to move perpendicular to the gravitational field. The flow along the adiabatic walls now can fill a larger area in

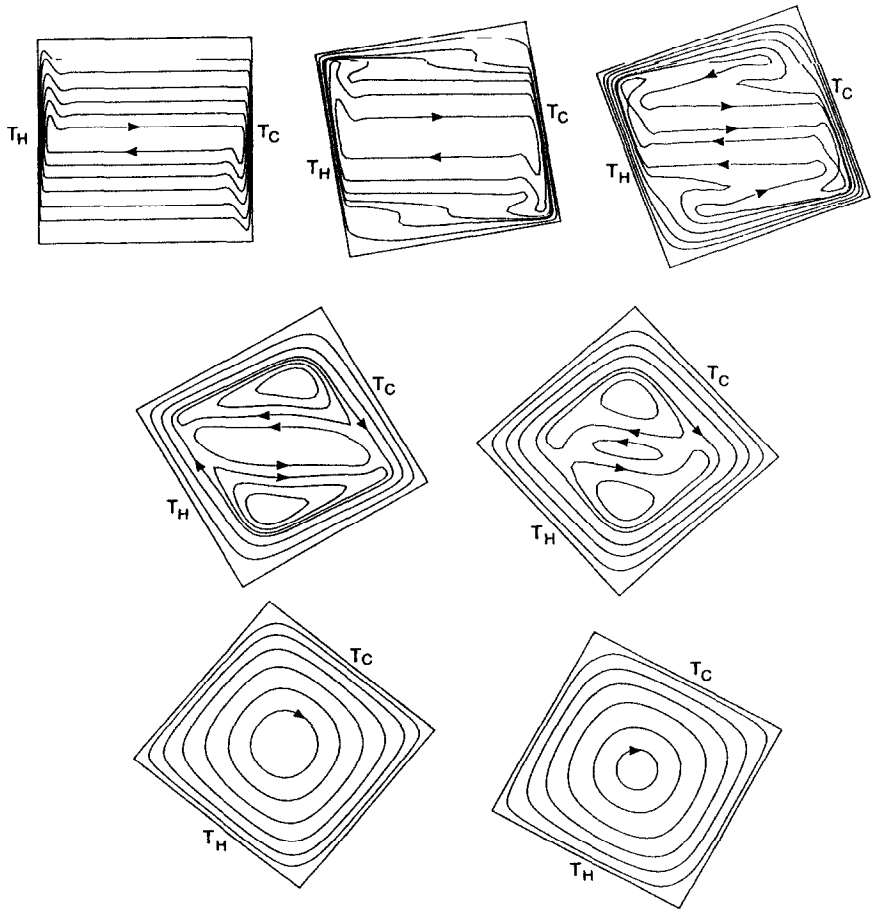

FIG. 6. Flow fields for $Ra = 10^{10}$. Plotted are some isolines of the streamfunction for $\varphi = 90°$, $\varphi = 80°$, $\varphi = 70°$, $\varphi = 60°$, $\varphi = 50°$, $\varphi = 40°$, $\varphi = 30°$.

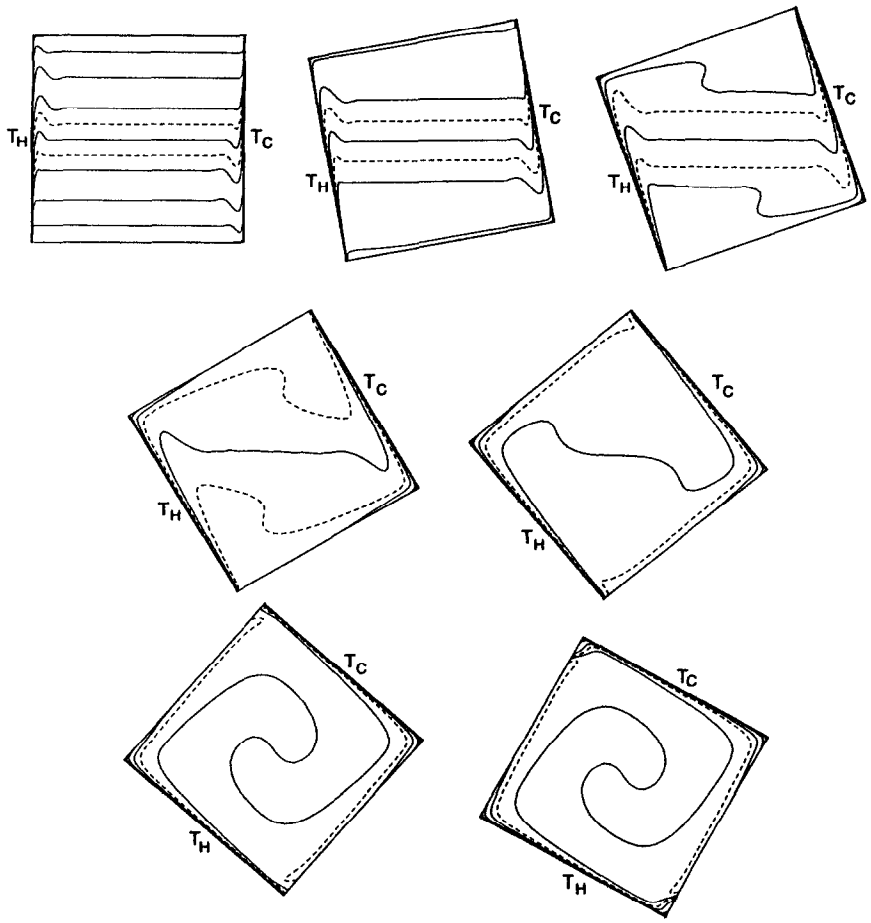

FIG. 7. Temperature distribution for $Ra = 10^{10}$. Plotted are isotherms $(T-T_C)/\Delta T = 0(0.1)1$ and $(T-T_C)/\Delta T = 0.45, 0.55$ in dotted lines at angles $\varphi = 90°$, $\varphi = 80°$, $\varphi = 70°$, $\varphi = 60°$, $\varphi = 50°$, $\varphi = 40°$, $\varphi = 30°$.

the corner regions and spreads as can be seen from the curving streamlines. This area is well mixed and almost isothermal.

At an angle of inclination of 70°, the flow is stratified in only a small part of the core region. The curvature of the streamlines along the adiabatic walls has enlarged; the fluid bounces back at the opposing walls and almost reaches the wall it left again, before moving back perpendicular to the gravitational field.

This meandering of the flow changes smoothly to a closed cell structure during rotation at an angle of inclination between 60 and 65°. The same velocity and temperature distribution appears as in the case of $Ra = 10^6$ and an angle of inclination of 50°. The core region temperature distribution now leads to a growth of the cells along the boundary layers instead of the centre cell as was the case in the laminar calculations.

At an angle of inclination of 45°, the two cells are closing in on this centre cell and a transition to a unicellular flow appears, as discussed later. At $\varphi = 30°$, the temperature distribution shows the birth of counterclockwise rotating cells at the start of the hot and cold wall boundary layers. This flow remains up to very small angles of inclination. We assume the mean flow to become three-dimensional at an angle close to 0°.

The calculations have been checked using the Dirichlet boundary conditions for the turbulence equations. The same flow and temperature distribution patterns appeared. The mean Nusselt number is compared with the previous calculated mean Nusselt number in Fig. 8. Although the level is higher, the same behaviour is found. The Nusselt number increases rapidly when rotating from an angle of inclination higher than 90° towards 90°. As soon as the flow becomes turbulent, the mean Nusselt number slowly increases to the transition point at $\varphi = 45°$. After a jump to a lower level, the growth in the heat transfer perseveres up to small angles. The curve behaves like a cosine function for angles of inclination close to 0° as was already found in previous laminar studies [5].

4.3.1. *Hysteresis.* During the rotation of a cavity containing the turbulently flowing fluid at $Ra = 10^{10}$

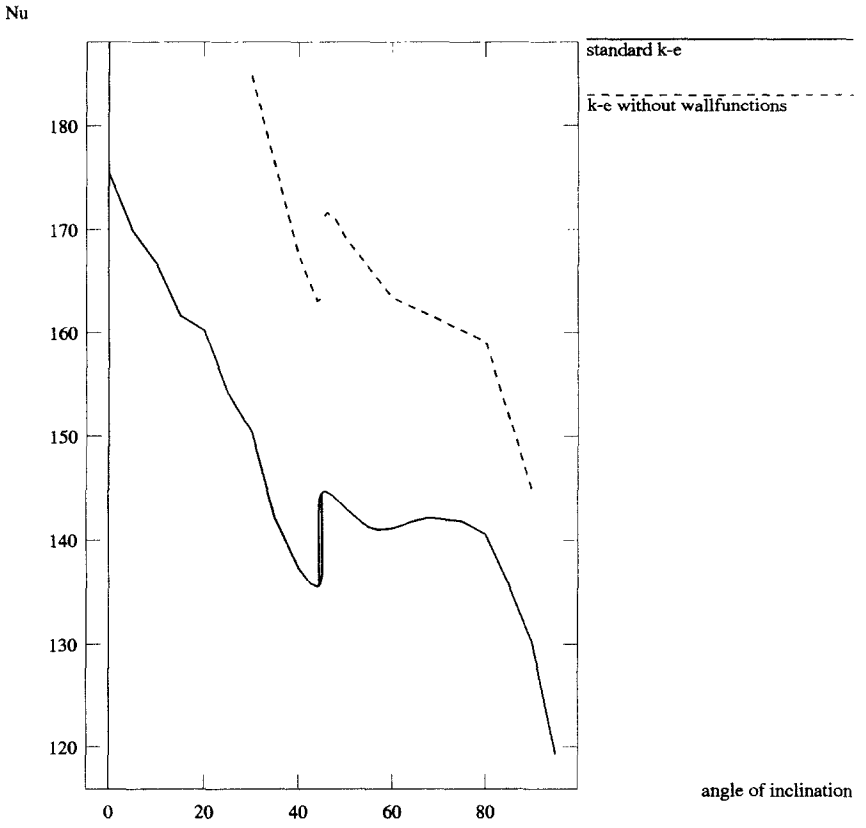

FIG. 8. Dependence of mean Nusselt number on angle of inclination for $Ra = 10^{10}$.

and $\varphi = 50°$, we saw the same patterns in flow structure and heat transfer as in the laminar case of $Ra = 10^6$ and $\varphi = 30°$. The transition to a unicellular flow at an angle of inclination of approximately 45° will not be related to the laminar–turbulent transition since turbulence is already sufficiently strong for angles of inclination larger than 45° in the problem for $Ra = 10^{10}$. Since the Rayleigh number is large the mean flow will be two-dimensional up to very small angles. We will discuss the results for the velocity field and the mean Nusselt number at $\varphi = 45°$ by going towards this angle from two sides as indicated in Figs. 9 and 10.

Approaching the angle of inclination of 45° from larger angles, the core region contains three cells. The rotation of these cells is oriented like tooth-wheels driven by the surrounding boundary layer flow. When the angle of inclination decreases, the flow along the adiabatic walls increases in strength and turbulence. The area occupied by this flow along the adiabatic walls broadens and the area available for the cells in the core region gets smaller. The clockwise rotating cells are squeezed towards each other and the cell in the centre of the cavity shrinks rapidly. As soon as the centre cell has completely vanished, the two 'tooth-wheels' start to interact on a smaller area, thereby producing large stresses. If the stresses become too large, the two cells melt into one cell, forming the unicellular flow at small angles.

Approaching this angle of transition from smaller angles, the unicellular flow will lose strength since the instability of the situation of a cavity heated from below is diminished. As the flow along the adiabatic walls slows down, it will dominate a smaller region of the cavity, thus producing an almost stagnant space in the core region. As soon as the produced space is large enough, the three cells will appear again, rotating like the original tooth-wheels.

In the discussion of the transition we can determine the mechanism being one of 'increasing tendency to change the flow structure'. In order to understand this tendency, the same effect can be seen by rotating a cavity through the point at which the angle of inclination equals 0° : coming from positive angles the flow will be clockwise, while coming from negative angles the flow will be counterclockwise. The existing flow pattern remains until a certain threshold is reached and then changes to the new mode of motion. Since the existing flow pattern persist, a hysteresis in the transition is found. Numerically, we found two solutions of the equations, depending on the initial field of the iteration process. If the initial field of the calculation at $Ra = 10^{10}$ contained three cells in the core region, this pattern remained until the angle of inclination was lowered to 44.3°. The unicellular motion remained up to an angle of 45°.

Grid refinement up to a 90×90 grid and Rayleigh number variation from $Ra = 10^9$ to 10^{11} were applied

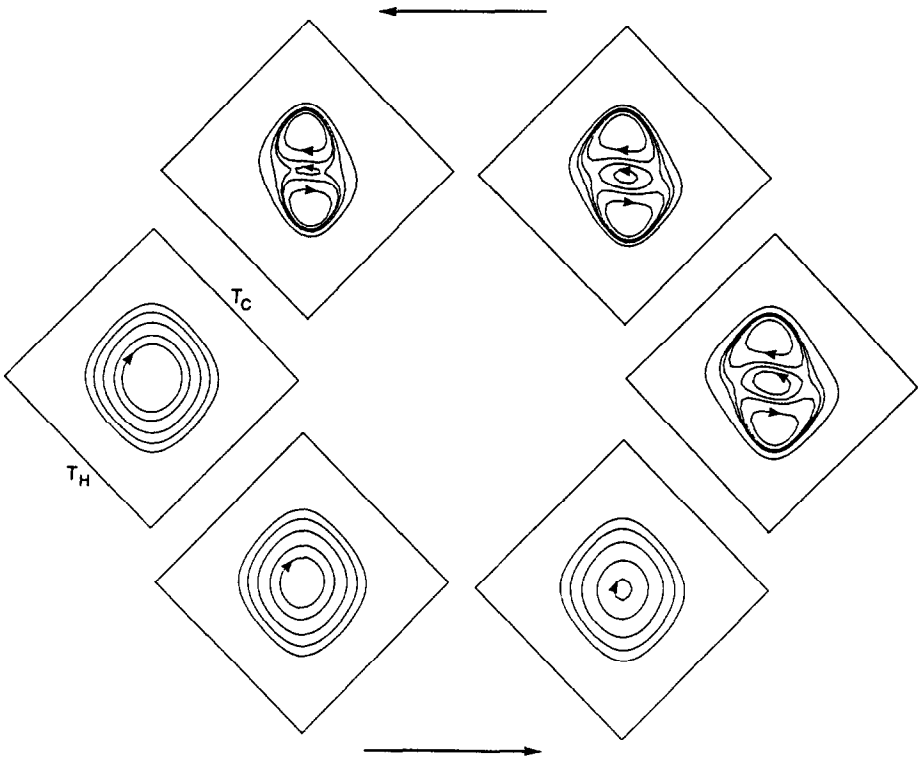

FIG. 9. Hysteresis in the solution of the flow field distribution. Plotted are streamlines in the core region. The lower results are obtained by approaching from lower angle, while the upper results are obtained by approaching from higher angle. From left to right the angle of inclination equals 44°, 44.4°, 44.7° and 45.1°.

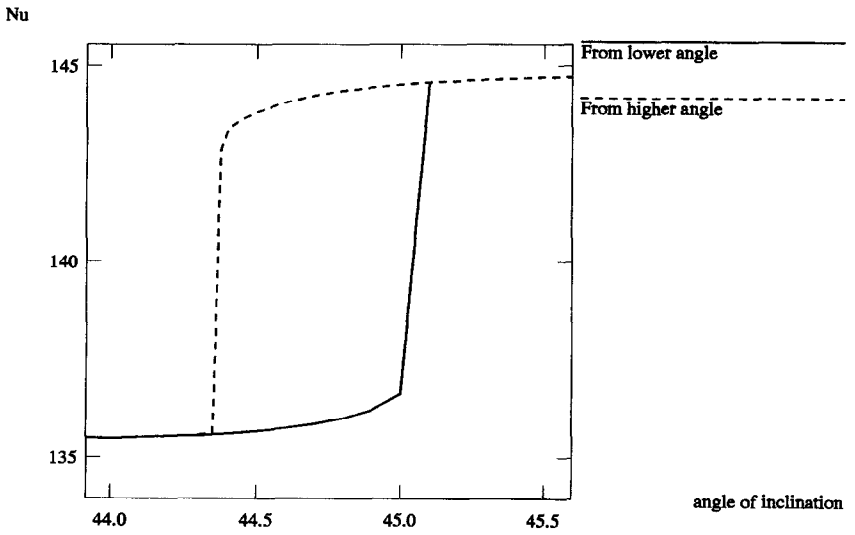

FIG. 10. Hysteresis loop in the mean Nusselt number.

to check the numerical dependency of the phenomenon. The angle at which the transition occurs depends on the Rayleigh number of the problem. For $Ra = 10^9$ the hysteresis was found at an angle of 42.5°, for $Ra = 10^{10}$ at 44.5° and for $Ra = 10^{11}$ at 45.5°. Since the angle at which the transition takes place is increasing with increasing Rayleigh number it is expected that the phenomenon is directly associated with the transition arising at an angle of inclination of 20° at $Ra = 10^6$.

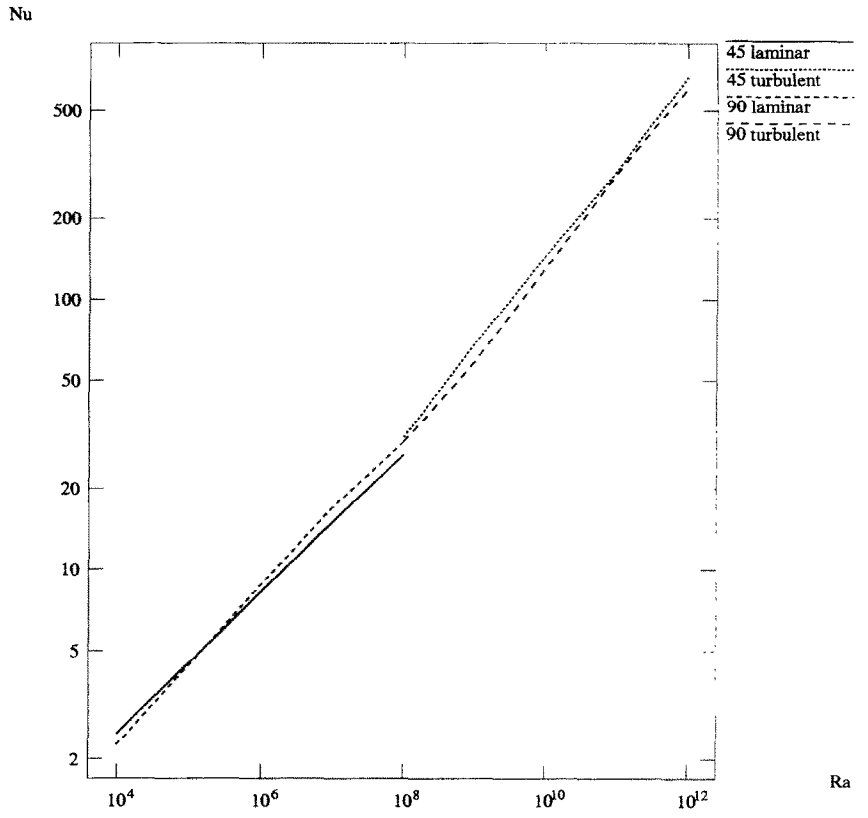

FIG. 11. Rayleigh number dependence of mean Nusselt number at angles of inclination of 45° and 90°.

4.4. *Rayleigh number dependence*

The dependence of the mean Nusselt number on the Rayleigh number has been examined for the cases $\varphi = 45$ and 90°. Figure 11 shows the results of the calculations, in which the transition to turbulence at a Rayleigh number of approximately 10^8 has been treated by calculating both a laminar and a turbulent solution. The mean Nusselt number can best be correlated to the Rayleigh number by

$$\overline{Nu} = \begin{cases} 0.231\,Ra^{0.258} & \text{for } Ra \leqslant 10^8 \text{ and } \varphi = 45° \\ 0.171\,Ra^{0.282} & \text{for } Ra \leqslant 10^8 \text{ and } \varphi = 90° \\ 0.069\,Ra^{0.332} & \text{for } Ra \geqslant 10^8 \text{ and } \varphi = 45° \\ 0.050\,Ra^{0.341} & \text{for } Ra \geqslant 10^8 \text{ and } \varphi = 90° \end{cases} \quad (8)$$

We can see that the coefficients of approximately 1/4 and 1/3 for the laminar and turbulent case respectively appear in the correlations for both angles of inclinations.

This shows that the results of the laminar calculations at $Ra = 10^6$ and the turbulent calculations at $Ra = 10^{10}$ can be extrapolated to other Rayleigh numbers in the same regime at all angles of inclination using the power law relation 8. However, care should be taken in cases where a transition of flow patterns is crossed.

5. CONCLUSIONS

Numerical calculations have been presented for the natural convection flow in an inclined square cavity at a wide variety of angles of inclination and Rayleigh numbers. The flow structures for both the laminar and turbulent flows have been discussed and show large similarity.

The results for the calculation of the mean Nusselt number as a function of the angle of inclination of the cavity have been presented. These results can be used to predict the heat transfer in a wide range of Rayleigh numbers belonging to the same flow regime. The results for the laminar case show agreement with results from previous studies, but since the results of previous studies differ on essential properties ($Nu = 1$ at $\varphi = 180°$, benchmark solution at $\varphi = 90°$), it can be concluded that the presented results are very reliable.

Turbulent calculations have been made for $Ra = 10^{10}$ at different angles of inclination. To the authors' knowledge this is the first thorough study dealing with an inclined cavity containing a turbulent natural convection flow. Results for the flow structures and temperature distribution have been discussed for all interesting angles of inclination of the cavity.

An interesting transition phenomenon, including a hysteresis in the solution, has been discussed in the

results for the turbulent flows. The structures involved in this transition, combined with the Rayleigh number dependence of the transition angle, indicates that this transition is related to the critical angle of inclination in laminar flow studies.

Acknowledgements—These investigations are supported by the Netherlands' Foundation for Chemical Research (SON) with financial aid from the Netherlands' Technology Foundation (STW).

REFERENCES

1. K. T. Yang, Transitions and bifurcations in laminar buoyant flows in confined enclosures, *J. Heat Transfer* **110,** 1191–1204 (1988).
2. I. Catton, Natural convection in enclosures, *Proc. Sixth Int. Heat Transfer Conf.*, Toronto, Canada, Vol. 6, pp. 13–31 (1978).
3. J. E. Hart, Stability of the flow in a differentially heated inclined box, *J. Fluid Mech.* **47,** 547–576 (1971).
4. H. Ozoe, H. Sayama and S. W. Churchill, Natural convection in an inclined rectangular channel at various aspect ratios and angles—experimental measurements, *Int. J. Heat Mass Transfer* **18,** 1425–1431 (1975).
5. J. N. Arnold, I. Catton and D. K. Edwards, Experimental investigation of natural convection in inclined rectangular regions of different aspect ratios, *J. Heat Transfer* **98,** 67–71 (1976).
6. S. M. Elsherbiny, K. G. T. Hollands and G. D. Raithby, Nusselt number distribution in vertical and inclined air layers, *J. Heat Transfer* **105,** 406–408 (1983).
7. S. J. M. Linthorst, W. M. M. Schinkel and C. J. Hoogendoorn, Flow structure with natural convection in inclined air-filled enclosures, *J. Heat Transfer* **103,** 535–539 (1981).
8. K. G. T. Hollands and L. Konicek, Experimental study of the stability of differentially heated inclined air layers, *Int. J. Heat Mass Transfer* **16,** 1467–1476 (1973).
9. H. Ozoe, H. Sayama and S. W. Churchill, Natural convection in an inclined square channel, *Int. J. Heat Mass Transfer* **17,** 401–406 (1974).
10. H. Ozoe, K. Yamamoto, H. Sayama and S. W. Churchill, Natural convection in an inclined rectangular channel heated on one side and cooled on the opposing side, *Int. J. Heat Mass Transfer* **17,** 1209–1217 (1974).
11. I. Catton, P. S. Ayyaswamy and R. M. Clever, Natural convection flow in a finite, rectangular slot arbitrarily oriented with respect to the gravity vector, *Int. J. Heat Mass Transfer* **17,** 173–184 (1974).
12. H. Ozoe, K. Fujii, N. Lior and S. W. Churchill, Long rolls generated by natural convection in an inclined rectangular enclosure, *Int. J. Heat Mass Transfer* **26,** 1427–1438 (1983).
13. Z. Y. Zhong, K. T. Yang and J. R. Lloyd, *Variable Property Natural Convection in Tilted Enclosures with Thermal Radiation* (Edited by R. W. Lewis and K. Morgan), Vol. 3, pp. 195–214. Wiley, New York (1985).
14. F. J. Hamady, J. R. Lloyd, H. Q. Yang and K. T. Yang, Study of local natural convection heat transfer in an inclined enclosure, *Int. J. Heat Mass Transfer* **32,** 1697–1708 (1989).
15. Y. E. Karyakin, Transient natural convection in prismatic enclosures of arbitrary cross-section, *Int. J. Heat Mass Transfer* **32,** 1095–1103 (1989).
16. T. S. Lee, Numerical experiments with fluid convection in tilted nonrectangular enclosures, *Numer. Heat Transfer* **19,** 487–499 (1991).
17. N. C. Markatos and K. A. Pericleous, Laminar and turbulent natural convection in a enclosed cavity, *Int. J. Heat Mass Transfer* **27,** 755–772 (1984).
18. S. Paolucci, Direct numerical simulation of two-dimensional turbulent natural convection in an enclosed cavity, *J. Fluid Mech.* **215,** 229–262 (1990).
19. A. Lankhorst, Laminar and turbulent natural convection in cavities: numerical modeling and experimental validation, Ph.D. Thesis, Delft University of Technology, Delft, The Netherlands (1991).
20. T. Nishimura, F. Nagasawa and Y. Kawarura, Natural convection heat transfer in inclined enclosures with/without partitions, *Proc. Ninth Int. Heat Transfer Conf.*, Jerusalem, Israel, Vol. 2, pp. 495–500 (1990).
21. D. D. Gray and A. Giorgini, The validity of the Boussinesq approximation for liquids and gases, *Int. J. Heat Mass Transfer* **19,** 545–551 (1976).
22. R. A. W. M. Henkes, Natural-convection boundary layers, Ph.D. Thesis, Delft University of Technology, Delft, The Netherlands (1990).
23. S. V. Patankar, *Numerical Heat Transfer and Fluid Flow*. Hemisphere, Washington (1980).
24. G. de Vahl Davis, Natural convection of air in a square cavity: a bench mark numerical solution, *Int. J. Num. Meth. Fluids* **3,** 249–264 (1983).